

# Dalton Transactions

Accepted Manuscript



This is an *Accepted Manuscript*, which has been through the Royal Society of Chemistry peer review process and has been accepted for publication.

*Accepted Manuscripts* are published online shortly after acceptance, before technical editing, formatting and proof reading. Using this free service, authors can make their results available to the community, in citable form, before we publish the edited article. We will replace this *Accepted Manuscript* with the edited and formatted *Advance Article* as soon as it is available.

You can find more information about *Accepted Manuscripts* in the [Information for Authors](#).

Please note that technical editing may introduce minor changes to the text and/or graphics, which may alter content. The journal's standard [Terms & Conditions](#) and the [Ethical guidelines](#) still apply. In no event shall the Royal Society of Chemistry be held responsible for any errors or omissions in this *Accepted Manuscript* or any consequences arising from the use of any information it contains.

# Halocuprate(I) Zigzag Chain Structures with *N*-Methylated DABCO Cations – Bright Metal-Centered Luminescence and Thermally Activated Color Shifts

Sebastian Maderlehner <sup>a‡</sup>, Markus J. Leitl <sup>b‡</sup>, Hartmut Yersin <sup>\*b</sup>, Arno Pfitzner <sup>\*a</sup>

<sup>a</sup> Institute for Inorganic Chemistry, University of Regensburg, Universitätsstraße 31, 93053 Regensburg, Germany. Fax: +49 941 943814551; Tel: +49 941 943 4551; E-mail: arno.pfitzner@chemie.uni-regensburg.de

<sup>b</sup> Institute for Physical Chemistry, University of Regensburg, Universitätsstraße 31, 93053 Regensburg, Germany. Fax: +49 941 9434488; Tel: +49 941 943 4464; E-mail: hartmut.yersin@chemie.uni-regensburg.de

<sup>‡</sup>These authors contributed equally to this work

**Abstract:** Two compounds 1,4-dimethyl-1,4-diazoniabicyclo[2.2.2]octane catena-tetra- $\mu$ -halocuprate(I) with DABCOMe<sub>2</sub> Cu<sub>2</sub>X<sub>4</sub> (**1**: X = Br, **2**: X = I) were synthesized by hydrothermal reaction of copper(I) halides with the corresponding 1,4-diazoniabicyclo[2.2.2]octane (DABCO) dihydrohalides in an acetonitrile/methanol mixture. Both compounds crystallize monoclinically, **1** with  $a = 9.169(4)$  Å,  $b = 10.916(6)$  Å,  $c = 15.349(6)$  Å,  $\beta = 93.93(2)^\circ$ ,  $V = 1533(1)$  Å<sup>3</sup>,  $Z = 4$ , space group  $P2_1/n$  (No. 14) and **2** with  $a = 15.826(9)$  Å,  $b = 9.476(5)$  Å,  $c = 22.90(2)$  Å,  $\beta = 90.56(5)^\circ$ ,  $V = 3434(5)$  Å<sup>3</sup>,  $Z = 8$ , space group  $P2_1$  (No. 4), respectively (lattice constants refined from powder diffraction data measured at 293 K). The cations in both compounds are formed by in-situ *N*-methylation of DABCOH<sub>2</sub><sup>2+</sup> cations by methanol in a  $S_N2$  reaction. Both compounds contain an anionic copper(I) halide chain structure consisting of trans edge-sharing CuX<sub>4</sub> tetrahedra. The chains are strongly kinked at every 2<sup>nd</sup> junction thus forming a zigzag structure. The shortest halide-halide distances are observed between the halide ions of adjacent tetrahedra which are approaching each other due to the kinking. This structure type shows a specific luminescence behavior. Under optical excitation, the compounds exhibit yellow (**1**) and green (**2**) emission with photoluminescence quantum yields of  $\Phi_{pl} = 52$  and 4 %, respectively, at ambient temperature. According to DFT and TDDFT calculations, the emission is assigned to be a phosphorescence essentially involving a metal centered transition between the HOMO consisting mainly of copper 3*d* and halide *p* orbitals and the LUMO consisting mainly of copper 4*s* and 4*p* orbitals. The temperature dependence of the emission spectra, decay times, and quantum yields has been investigated in detail, especially for **1**. From the resulting trends it can be concluded that the emission for  $T \leq 100$  K stems from energetically lower lying copper halide segments. Such segments represent the structure motif of the halocuprate(I) chains. With increasing temperature energetically higher lying segments are populated which also emit, but open the pathway for thermally activated energy transfer to quenching defects.

## Introduction

Halocuprates(I) are built from a very small number of building blocks which is in contrast to their structural diversity. One of these building blocks is the CuX<sub>4</sub>-tetrahedron ( $X = \text{Cl, Br, I}$ ). All types of linkage between tetrahedral units are observed including face-sharing with

Cu-Cu distances shorter than in metallic copper.<sup>1,2</sup> This diversity is one reason for the rich structural chemistry of such materials. In case of  $[\text{P}(\text{C}_6\text{H}_5)_4]_2[\text{Cu}_2\text{I}_4]$ , four different polymorphs are known which contain two different conformers of the  $[\text{Cu}_2\text{I}_4]^{2-}$  anion<sup>3,4</sup> and recently, a solvate of a tetraphenylphosphonium iodocuprate(I) containing acetone as solvent molecules was reported<sup>5</sup>. Furthermore, another tetraphenylphosphonium iodocuprate(I) containing a polyanion forming a helix built from CuI<sub>4</sub>-tetrahedra has been reported.<sup>6</sup> A quite common structural motif in catena-cuprates(I) is a chain of trans edge-sharing tetrahedra. Several halocuprates(I) with this anionic structural feature are described in the literature.<sup>7-15</sup> Typical cations are alkali metals, ammonium, or even copper(II) which is coordinated by four ammine<sup>7</sup> or two bidentate ethylenediamine ligands<sup>8-10</sup>. The same complex anion containing trans edge-sharing tetrahedra was obtained with twofold protonated diamines such as ethylene diamine or piperazine as cations.<sup>11</sup> Bromocuprates(I) with similar structures were obtained with *N*-allylquinolinium<sup>12</sup>, *N*-allylmorpholinium<sup>13</sup>, 4-aminopyridinium<sup>14</sup>, and 2,6-diaminopyridinium<sup>15</sup> cations, respectively. All of these compounds can be classified into two groups depending on the arrangement of the tetrahedra within the halocuprate(I) complex anions, i.e. as stretched form, similar to the chains of tetrahedra in silicon disulfide<sup>16,17</sup>, and as kinked chain at every 2<sup>nd</sup> junction causing a zigzag structure of the chain. An inverted chain structure with an N<sup>3-</sup> anion in the center of the tetrahedra has been observed in lanthanide nitride halides<sup>18,19</sup>, lanthanide nitride tellurides<sup>20</sup> and alkali metal lanthanide halide tellurides<sup>21</sup>. Stretched anti-Si<sub>2</sub> chains are observed within these compounds as well as the kinked ones.

In-situ *N*-alkylation of DABCO or other amines by methanol has been observed in high pressure experiments<sup>22</sup> and hydrothermal syntheses<sup>23-25</sup>, respectively. The use of DABCO and its protonated forms in halocuprate(I) syntheses has yielded a Cu<sub>4</sub>I<sub>6</sub><sup>2-</sup> cluster with an in-situ mono-methylated DABCO molecule<sup>25</sup>, and a 3D inorganic framework structure<sup>26</sup>. The crystal structure of **2** has recently been reported in a very brief form.<sup>27</sup> Structural data with higher quality are included in this paper.

The structural variability of halocuprates(I) and copper(I) halide clusters results in a rich diversity also in the luminescence properties, as many compounds emit visible light in different spectral regions upon optical

excitation.<sup>28-42, 104, 105</sup> Although many studies have been performed during recent years on the emission behavior of Cu(I) complexes due to their potential for use as low-cost emitter materials for OLEDs<sup>36-45,100-104</sup>, only very limited investigations in this regard were carried out on copper-halide chains, such as the ones presented in this contribution.<sup>46-48, 105, 107-109</sup>

Herein, the syntheses, crystal structures, and photophysical properties of two new luminescent halocuprate(I) compounds containing chains of trans edge-sharing tetrahedra are presented and discussed. This structure type is connected with the occurrence of specific chain segments which largely determine the emission behavior as is elucidated, in particular, for compound **1**. Photophysical characterizations are carried out on the basis of detailed temperature-dependent studies of emission spectra, decay times, and quantum yields. DFT and TDDFT calculation were performed to complement the measurements. It was found that at low temperature the emission originates only from one type of chain segments. With increasing temperature, thermally activated energy transfer along the chain occurs to other chain segments and quenching states.

## Experimental

[DABCOMe<sub>2</sub>][Cu<sub>2</sub>Br<sub>4</sub>] (**1**) and [DABCOMe<sub>2</sub>][Cu<sub>2</sub>I<sub>4</sub>] (**2**) were synthesized in a hydrothermal reaction. The freshly purified copper(I) halide<sup>49</sup> and DABCO dihydrobromide<sup>50</sup> or DABCO dihydroiodide monohydrate<sup>51</sup>, respectively, were weighed in a silica ampoule in a 1.8 : 1 ratio to achieve full conversion of the copper(I) halide. A typical reaction mixture contained 170 mg of the copper(I) halide and 180 mg (**1**) or 191 mg (**2**), respectively, of the corresponding DABCO dihydrohalide. Methanol (2.5 equivalents referring to DABCO·2HX (X = Br, I) and 1.5 mL acetonitrile were added as solvent. The ampoules were evacuated and sealed after freezing of the solvent with liquid nitrogen and were then transferred into a micro autoclave containing 5 mL of water to apply counter pressure. The reactions were performed at 150 °C for 5 days (**1**) or 130 °C for 14 days (**2**), respectively, yielding a pure product of colorless rod-like crystals in a 90% isolated yield referring to the amount of copper(I) halide. The rest of copper(I) halide remained in solution. Crystals suitable for single crystal X-ray structure determination were mounted on and glued to a glass fiber.

Diffraction data of **1** were collected on a STOE IPDS I (Mo-K<sub>α</sub>, λ = 0.71073 Å) at room temperature. Data were corrected for Lorentz and polarization effects and absorption was corrected numerically after a semi empirical optimization of the crystal shape.<sup>52</sup> The structure was solved by direct methods using SIR92<sup>53</sup> followed by a full-matrix least-squares refinement with SHELXL97<sup>54</sup>. Hydrogen atom positions could be located from difference Fourier calculations and were refined without constraints but fixed  $U_{\text{iso}} = 0.035 \text{ \AA}^2$  for methylene group protons and  $0.050 \text{ \AA}^2$  for methyl group protons, respectively.

Diffraction data of **2** were collected on an Xcalibur

Ruby Gemini Ultra (Mo-K<sub>α</sub>, λ = 0.71073 Å) at 123 K. Data were corrected for Lorentz and polarization effects and a numerical absorption correction was performed after semi empirical optimization of the crystal shape.<sup>55</sup> Solution and refinement of the structure were performed analogously to **1**. Hydrogen atoms were attached to the carbon atoms and refined with a riding model (HFIX 23 for methylene groups) and with circular Fourier (HFIX 137 for methyl groups), respectively. An isotropic displacement parameter  $U_{\text{iso}}(\text{H})$  of  $1.2 U_{\text{eq}}(\text{C})$  ( $1.5 U_{\text{eq}}(\text{C})$  for methyl group hydrogens) was constrained for the hydrogen atoms.<sup>54</sup> The single crystal used for data collection turned out to be twinned according to the matrix (-1 0 0, 0 -1 0, 0 0 1), i.e., a twofold axis along *c*. Both domains showed racemic twinning due to the chiral space group. Proportions of the 4 domains refined to 45.6% for the main domain, 43.5% for the 2<sup>nd</sup> domain, 5.5% for the racemic twin of the main domain, and 5.4 % for the racemic twin of the 2<sup>nd</sup> domain, respectively. Anisotropic refinement of carbon and nitrogen atoms did not provide any reasonable results. For this reason they were refined only with isotropic displacement parameters. Further crystallographic data and refinement details are displayed in Table 1.

Powder diffraction patterns of **1** and **2** were collected on a STOE STADI P (Cu-K<sub>α1</sub>, λ = 1.540598 Å) to confirm purity of the products, see supporting information Figures S1 and S2. IR spectra of the products and the DABCO dihydrohalides were collected on a Varian Fourier transform Raman Module coupled to a Varian 670 IR-FT-IR spectrometer using ATR technique to approve quantitative twofold *N*-methylation of the DABCO molecules within **1** and **2**, see supporting information Figures S3 and S4. The IR-spectra were processed with the Varian Resolutions Pro software.<sup>56</sup> NHC elemental analyses were performed on a Vario micro cube Elementaranalysensysteme GmbH and match the calculated values very well: **1** calculated: N 4.8%, H 3.1%, C 16.3%; found: N 4.8%, H 3.0%, C 16.5%; **2** calculated: N 3.6%, H 2.3%, C 12.4%; found: N 3.5%, H 2.3%, C 12.5%.

Emission and excitation spectra were recorded using a Fluorolog 3-22 (Horiba Jobin Yvon) spectrometer. Emission decay times were measured with a cooled photomultiplier (RCA C7164R) combined with a FAST ComTec multichannel scaler PCI card. For excitation, a pulsed Nd:YAG laser (λ<sub>exc</sub> = 355 nm) was used and the signal was detected at the respective emission maximum. The temperature dependent measurements between 10 and 300 K (emission spectra and decay times) were recorded using a helium cryostat (Cryovac Konti Cryostat IT). For absolute measurements of the photoluminescence quantum yields, a Hamamatsu Photonics (C9920-02) system was used. For this, the excitation wavelength was set to λ<sub>exc</sub> = 350 nm. DFT and TDDFT calculations were performed using the Gaussian09 software package. For all calculations, the basis set LANL2DZ with an effective core potential was applied along with the B3LYP hybrid functional. The calculations were performed using the geometry obtained from X-ray diffraction measurements without further

optimization.

## Results and Discussion

### Crystal Structures

The compounds **1** and **2** contain the tetra- $\mu$ -halocuprate(I) polyanion consisting of exclusively edge-sharing  $\text{CuX}_4$ -tetrahedra ( $X = \text{Br}, \text{I}$ ). These chains of tetrahedra are strongly kinked at every 2<sup>nd</sup> junction in **1** and **2** thus forming zigzag chains. The chains are arranged along [0 1 0] in **1** and along [0 0 1] in **2**, respectively, forming a hexagonal rod packing in both compounds. In **1**, all chains have the same alignment and are in an almost eclipsed conformation parallel to the chain direction. In contrast in **2**, the chains are arranged in an ABAB stacking along [1 0 0] and show a significant staggering parallel to the chain direction, see Figure 1. The staggering causes a doubling of the translation period of the chains in **2**, see Table 1. The crystallographic data given in Table 1 show some clear differences between the compounds under discussion. This holds regardless the fact that they contain the same cation and very similar polyanions. The lower symmetry of **2** is manifested by the staggering of the polyanions therein. This results in a symmetry reduction of the centrosymmetric space group  $P2_1/n$  of **1** to the acentric space group  $P2_1$  of **2** in combination with a doubling of the unit cell volume.

((Insert Figure 1 here))

((Insert Table 1 here))

As mentioned above, a chain of tetrahedra kinked at every 2<sup>nd</sup> junction has already been reported in literature.<sup>7,12,20,27</sup> It was observed in the *N*-allylquinolinium bromocuprate(I)<sup>12</sup>, in the rubidium and ammonium iodocuprate(I) hydrates<sup>7</sup> and in the rare earth (*RE*) nitride tellurides  $\text{RE}_4\text{N}_2\text{Te}_3$  ( $RE = \text{La-Nd}$ )<sup>20</sup>. The diammonium and dirubidium bis(di- $\mu$ -iodo-cuprate(I)) hydrates<sup>7</sup> show a kinking comparable to that in **1** and **2**. Within the former, the distances  $d(\text{I-I})$  between adjacent  $\text{CuI}_4$ -tetrahedra are shorter than some of the intra-tetrahedral distances  $d(\text{I-I})$ . The strong kinking results in short distances  $d(\text{Cu-Cu})$  in the ammonium and rubidium iodocuprates(I)<sup>7</sup> as well as in the title compounds. The shortest distances of  $d(\text{Cu-Cu}) = 2.809(3)$  Å in  $[(\text{NH}_4)_2(\text{H}_2\text{O})][\text{Cu}_2\text{I}_4]^7$  and  $d(\text{Cu-Cu}) = 2.897(3)$  Å in  $[\text{Rb}_2(\text{H}_2\text{O})][\text{Cu}_2\text{I}_4]^7$  are slightly longer than the sum of the van-der-Waals radii<sup>57</sup> of 2.8 Å, whereas the shortest distances of  $d(\text{Cu-Cu}) = 2.740(2)$  Å in **1** and  $d(\text{Cu-Cu}) = 2.679(0)$  Å in **2** are significantly shorter. All these distances are longer than the distance  $d(\text{Cu-Cu})$  of 2.556 Å in metallic copper<sup>58</sup>. This is not surprising since only those iodocuprates(I)<sup>59-61</sup> and bromocuprates(I)<sup>62</sup> containing face-sharing  $\text{CuX}_4$ -tetrahedra ( $X = \text{Br}, \text{I}$ ) show distances  $d(\text{Cu-Cu})$  in the range from 2.45 to 2.50 Å which are shorter than in metallic copper<sup>58</sup>. Structural details for the different halocuprates(I) and for  $\text{La}_4\text{N}_2\text{Te}_3$  (as a representative for the *RE*-nitride tellurides) are given in Table 2.

((Insert Table 2 here))

((Insert Figure 2 here))

The chains in **1** and **2** show the strongest kinking in the series of compounds displayed in Table 2, since the

shortest distances  $d(X-X)$  are observed between neighboring  $\text{CuX}_4$ -tetrahedra at the kinked junctions. A closer look at the angles  $\angle(X-\text{Cu}-X)$  and at the intra-tetrahedra distances  $d_{\text{edge}}(X-X)$  reveals significant distortions from an ideal tetrahedron within all compounds. The strongest distortion is found in the *N*-allylquinolinium compound due to a stretching of the bromocuprate(I) chain along the chain<sup>12</sup>. The dihedral angle between the faces of two undistorted edge-sharing tetrahedra should lie in the range from 66.0 to 70.5° to avoid distances  $d(X-X)$  at the kinking shorter than the intra-tetrahedron distances<sup>63</sup>. The dihedral angle between the faces is 62.0° in **1** and 62.1-63.3° in **2**.

The title compounds contain twofold *N*-methylated DABCO cations which take a staggered conformation with dihedral angles  $\angle(\text{N-C-C-N})$  of 14.8-16.5° in **1** and 0.8-16.4° in **2**, respectively. The cations are embedded between the anionic halocuprate(I) chains with each cation next to an almost planar face of a kinked junction, see Figure 3. This figure shows that the space required by the cations matches the size of the plain face of the kinked tetrahedra junction quite well. In **1**, the cations have only one orientation with a small tilt of the N-N axis apart from the chain direction while in **2** the cations show two different orientations. One of them is similar to the orientation of the cations in **1** with a stronger tilt of the N-N axis. The second orientation is almost parallel to the chain direction, see Figure 3. The tilted cations in **2** have a stronger staggered conformation with dihedral angles  $\angle(\text{N-C-C-N})$  of 10.0-16.4° than those oriented parallel to the chains with dihedral angles  $\angle(\text{N-C-C-N})$  of 0.8-4.5°.

((Insert Figure 3 here))

The cations are formed by an in-situ di-methylation of DABCO by methanol which is possible due to the enhanced pressure during the hydrothermal reaction, see Scheme 1.

((Insert Scheme 1 here))

It is well known that the size or volume per charge of the cation has a strong influence on the size and shape of the halocuprate(I) complex anion.<sup>1,2,64</sup> Sometimes choosing a particular cation allows for the prediction of the anionic structure.<sup>65</sup> The  $\text{DABCOMe}_2^{2+}$  cations in **1** and **2** have a quite high charge density. The two positive charges of the molecular cation are located at the nitrogen atoms and are therefore very close to each other with distances  $d(\text{N-N})$  of 2.56 Å in **1** and of 2.51 and 2.57 Å in **2**, respectively. Halocuprates(I) containing chains of edge-sharing  $\text{CuX}_4$ -tetrahedra have one negative charge per tetrahedral unit. This means that each copper atom in **1** and **2** can be assigned to an adjacent nitrogen atom of the cation providing electroneutrality. The kinking of the junction might be a result of the short distances between the charges of the cations. A stretched  $\text{Cu}_2\text{X}_4$ -chain would lead to a reduced electrostatic interaction of the complex anion and the assigned cations.<sup>66</sup> Thus, the structure of the anion in **1** and **2** is mostly determined by the cations.

### Photophysical properties

At ambient temperature, powders of the investigated compounds exhibit yellow (**1**) and green (**2**) luminescence, respectively, under optical excitation. The

corresponding emission spectra along with the excitation spectra are depicted in Figure 4. The emission of compound **1** peaks at 550 nm, while it is significantly blue-shifted for compound **2** with a maximum at 510 nm. The emission decay times amount to  $\tau = 86 \mu\text{s}$  (**1**) and  $\tau = 2.6 \mu\text{s}$  (**2**), respectively. For the emission quantum yields  $\Phi_{\text{PL}}$  values of 52 % (**1**) and 4 % (**2**) were found.

((Insert Figure 4 here))

In the following discussion, we will focus on compound **1**. DFT and TDDFT calculations were performed to get an insight into the nature of the electronic transition(s) responsible for the luminescence. All calculations were restricted to segments of the copper halide chain which contain 2 copper and 4 bromide atoms. In this rather crude model, the periodicity of the system is neglected. From Figure 2 (compare also Figure 6, below), it can be seen that there are two types of such  $\text{Cu}_2\text{Br}_6$  segments. In one type, the central copper and bromide atoms are arranged in a butterfly like shape (butterfly type, **A**) whereas in the other segment type these atoms are located in one plane (planar type, **B**). From the calculations it was found that the HOMOs for both types are located at the copper and bromide atoms, more specifically, the largest contributions to the HOMO stem from Cu  $3d$  orbitals (~60% (**A**), ~70% (**B**)) and Br  $4p$  orbitals (~15% (**A**), ~20% (**B**)). The LUMOs are mainly located on the copper atoms with the largest contributions stemming from  $4s$  orbitals (~55% (**A**), ~60% (**B**)). TDDFT calculations reveal that mainly transitions between the frontier orbitals determine the first excited singlet ( $S_1$ ) and triplet ( $T_1$ ) states for both types of segments. Moreover, as the emission decay time at ambient temperature is of the order of almost  $10^2 \mu\text{s}$ , the corresponding transition is assigned to be mainly metal-centered phosphorescence ( $^3(\text{MC})$ ) (with distinct halide contributions to the HOMO). The ground state is a singlet. This is in agreement with literature assignments of other, however molecular, halide copper systems.<sup>28-35,46,67</sup> Interestingly, the calculations give different transition energies for the  $T_1$  states for the two segments differing by about  $10^3 \text{ cm}^{-1}$  (0.12 eV), with segment **A** being the energetically lower one.

The strong involvement of the Cu  $3d$  orbitals in the HOMO might serve as an explanation for the observed blue shift of about 40 nm of the emission of compound **1** compared to that of **2**: The smaller ligand field strength of iodide compared to bromide results in a smaller splitting of the occupied Cu  $3d$  orbitals. As a consequence, the HOMO of **1** is more destabilized than the HOMO of **2**. Thus, the emission of **1** appears at lower energy. Indeed, such a destabilization of the HOMO is also confirmed by the DFT calculations. Similar shifts of the emission energies have also been reported for other copper halide systems.<sup>36,37,39</sup>

For a more detailed understanding of the emission behavior, the samples were cooled to 10 K. With decreasing temperature, a significant *unsymmetrical* narrowing of the emission spectrum occurs for compound **1**. Formally, the emission spectrum is red-shifted from 545 to 575 nm (peak to peak) which is equivalent to about  $960 \text{ cm}^{-1}$  (0.12 eV), see Figure 5. Interestingly, this

energy difference is of about the same size as the one estimated from the TDDFT calculations for the transition energies of the two chain segments **A** and **B**. Therefore, it is indicated that at low temperature the emission originates from the chain segment which exhibits the lower transition energy. In the case of compound **1**, this is segment **A**. With increasing temperature, a thermal activation of segment **B** becomes possible, compare Figure 6. Accordingly, a blue-shift and an *unsymmetrical* broadening of the emission spectrum are expected to occur upon heating. Indeed, this is observed experimentally. It is mentioned that in a recent report, a similar situation was described for a copper cyanide chain where the occurrence of different emission energies was also attributed to the existence of different chain segments.<sup>48</sup>

((Insert Figure 5 here))

Moreover, the emission decay time of compound **1** was also investigated in dependence of temperature, see Figure 7. Between 50 and about 100 K it amounts to about 180  $\mu\text{s}$ . With further temperature increase, the decay time decreases and reaches 86  $\mu\text{s}$  at 300 K. Additionally, the quantum yields at 77 and 300 K were measured to  $\Phi_{\text{PL}}(77 \text{ K}) = 85\%$  and  $\Phi_{\text{PL}}(300 \text{ K}) = 52\%$ . This allows us to determine the radiative rates according to  $k_r = \Phi_{\text{PL}}\tau^{-1}$ . Within experimental error, the radiative rates  $k_r$  at 77 and 300 K ( $k_r(77\text{K}) = 5 \cdot 10^3 \text{ s}^{-1}$ ,  $k_r(300\text{K}) = 6 \cdot 10^3 \text{ s}^{-1}$ ) are equal. Therefore, the observed decrease of the emission decay time is a consequence of an increase of the nonradiative rate. This behavior can be rationalized by two different quenching mechanisms which are schematically displayed in Figure 6. If the temperature is high enough, a thermally activated energy transfer between the chain segments can occur, presumably over a larger number of segments.<sup>a</sup> If so, the emission can be quenched by defects in the chain structure (see Figure 6, right-hand side).<sup>b</sup> Moreover, **B**-type chain segments themselves can exhibit an additional non-radiative decay channel to the ground state which becomes effective on thermal activation of these chain segments (see Figure 6, left-hand side). Also, a combination of both effects can

<sup>a</sup> Cu(I) complexes often undergo distortions on excitation which leads to a trapping of the excitation energy on one specific emitter molecule and therefore, prohibits an efficient energy transfer to adjacent molecules.<sup>36,37,39,43-45</sup> In the case of the compounds presented in this contribution, it seems that this self-trapping mechanism and therefore the localization of the excitation energy at one chain segment is not effective (at ambient temperature) for two reasons. (i) Distortions in molecular Cu(I) complexes on excitation are related to a pronounced charge-transfer from the copper center to the ligand. This leads to a formal oxidation of the copper center and therefore to a geometry change from a pseudo-tetrahedral towards a more planar geometry. For the copper halide chains presented in this study the transitions are mainly metal-centered and therefore, charge-transfer and geometry distortions do not seem to be significant. (ii) Possible geometry distortions are further reduced as the emitting individual chain segments are embedded into the rigid framework of the entire chain.

<sup>b</sup> Defects might be represented by defects in the chain structure itself, boundary effects, or unavoidable impurities in real systems. Energy transfer along the chain is presumably occurring by a Dexter energy transfer process. A corresponding quenching mechanism was already suggested by Dexter and Schulman.<sup>106</sup>

occur.

Thermally activated processes can (in the case of fast thermal equilibration) be described by modified Boltzmann functions which are often found in the literature.<sup>36,43-45</sup> Equation (1) represents an adaption of such a function to the system investigated in this contribution. Fitting this equation to the experimental data of decay time versus temperature, as shown in Figure 7, allows us to estimate the activation energy for the quenching processes.

((insert equation 1))

Herein,  $\Delta E(A-B)$  represents the energy difference between segment **A** and **B** and therefore, the activation energy for the energy transfer,  $\tau(A)$  and  $\tau(B)$  the emission decay times of segment A and segment B, respectively,  $\tau(D)$  the quenching constant for the non-radiative deactivation (via energy transfer to defect sites and quenching at segment B), and  $k_B$  the Boltzmann constant. For this rough approach we assume that the population of segment B and the quenching process exhibit the same activation energy, as a determination of the rate constants of the individual processes of segment **B** and of the defect site D is not possible in the scope of our experiments.<sup>c</sup>

From fitting the data displayed in Figure 7 with equation (1) it is found that the activation energy amounts to about  $1300\text{ cm}^{-1}$  (0.16 eV). This value is in reasonable agreement with the values determined for the energy difference between the two segments by the TDDFT calculations ( $\sim 10^3\text{ cm}^{-1}$ ) and the shift of the emission energy with temperature ( $\sim 960\text{ cm}^{-1}$ , Figure 5). Further support for this model is given by the fact that the decrease of the emission decay time is paralleled by the broadening of the emission spectra above  $T \sim 100\text{ K}$ . Therefore, it is not unreasonable to assume that both effects are caused by the same activation mechanism.

((Insert Figure 6 here))

((Insert Figure 7 here))

For completeness, it is mentioned that the observed decrease of the emission decay time with increasing temperature is not in agreement with a thermally activated delayed fluorescence (TADF) which is often found for molecular copper compounds, as the decrease found here is a result of a thermally activated quenching mechanism in contrast to the population of a highly emissive singlet state in the TADF case.<sup>36,37,39,43-45</sup>

## Conclusions

Two halocuprates(I) 1,4-dimethyl-1,4-diazoniabicyclo[2.2.2]octane *catena*-tetra- $\mu$ -halocuprate(I) with DABCOMe<sub>2</sub> Cu<sub>2</sub>X<sub>4</sub> (**1**: X = Br, **2**: X = I) have been synthesized and characterized by single crystal X-ray diffraction and luminescence spectroscopy. The use of methanol as a high pressure methylation agent yields twofold *N*-methylated DABCO cations formed in an in-situ *S<sub>N</sub>2*-reaction similar to reactions under extreme conditions reported in literature.<sup>22-25</sup> The influence of the

cation size on the structure of the halocuprate(I) anion becomes obvious from their crystal structures: A polyanion built of edge-sharing CuX<sub>4</sub>-tetrahedra (X = Br, I) is formed due to the high charge density of the DABCOMe<sub>2</sub><sup>2+</sup> cation. This is in perfect agreement to the tendency that highly charged cations yield polymeric halocuprate(I) anions with tetrahedrally coordinated copper atoms.<sup>1,2</sup>

Luminescence properties of both compounds were examined in detail. It was found that the emission results largely from a metal centered phosphorescence with distinct contributions of the halides to the HOMO. An analysis of the temperature dependence of the emission spectra, quantum yields, and of the decay time suggests for compound **1** that at low temperature the emission originates only from an energetically lower lying segment of the [DABCOMe<sub>2</sub>][Cu<sub>2</sub>Br<sub>4</sub>] chain, while with temperature increase energy states of an energetically higher lying segment are populated. This opens the pathway for an energy transfer along the chain but also for non-radiative deactivation channels either at the higher energy segments themselves or by energy transfer to defect sites. The activation energy for this process was determined to be in the range of  $1000 - 1300\text{ cm}^{-1}$  (0.12 – 0.16 eV).

## Acknowledgement

We gratefully acknowledge funding by the German Ministry of Education and Research (BMBF) in the scope of the cyCESH project (FKN 13N12668).

## Notes

Electronic Supplementary Information (ESI) available: IR spectra of **1**, **2**, DABCOH<sub>2</sub>Br<sub>2</sub> and DABCOH<sub>2</sub>H<sub>2</sub>O; Experimental and simulated powder diffraction patterns of **1** and **2**.

## References

- 1 C. Hasselgren Arnby, S. Jagner, I. Dance, *CrystEngComm*, 2006, **46**, 257.
- 2 S. Jagner, G. Helgesson, *Adv. Inorg. Chem.* 1991, **37**, 1.
- 3 H. Hartl, I. Brüdgam, F. Mahdjour-Hassan-Abadi, *Z. Naturforsch.* 1985, **40b**, 1032.
- 4 A. Pfitzner, D. Schmitz, *Z. Anorg. Allg. Chem.* 1997, **623**, 1555.
- 5 E. Jalilian, R.-Z. Liao, F. Himo, H. Brismar, F. Laurell, S. Lidin, *CrystEngComm*, 2011, **13**, 4729.
- 6 H. Hartl, F. Mahdjour-Hassan-Abadi, *Angew. Chem.* 1994, **106**, 1929; H. Hartl, F. Mahdjour-Hassan-Abadi, *Angew. Chem. Int. Ed. Engl.* 1994, **33**, 1841.
- 7 M. Hoyer, H. Hartl, *Z. anorg. allg. Chem.* 1991, **598/599**, 151.
- 8 R. P. Hammond, D. J. Chesnut, J. A. Zubieta, *J. Solid State Chem.* 2001, **158**, 55.
- 9 B. Freckmann, K. F. Tebbe, *Z. Naturforsch.* 1980, **35b**, 1319.
- 10 O. Simonsen, H. Toftlund, *Acta Crystallogr.* 1987, **e43**, 831.
- 11 E. Redel, M. Fiederle, C. Janiak, *Z. anorg. allg. Chem.* 2009, **635**, 1139.
- 12 A. V. Pavlyuk, V. N. Davydov and M. G. Mys'kiv, *Koord. Khim.* 2003, **29**, 199.
- 13 E. A. Goreschnik, M. G. Mys'kiv, *Koord. Khim.* 2003, **29**, 541.
- 14 J. Sertucha, A. Luque, F. Lloret, P. Román, *Polyhedron*, 1998, **17**, 3875.

<sup>c</sup> The degeneracy of the deactivating state(s) is not known and therefore, it is set to 1 in this rough estimate. Such a degeneracy factor has significant influence on the emission decay time but only minor influence on the activation energy. Therefore, only the activation energy is estimated.

- 15 S.-H. Liu, J.-D. Chen, L.-S. Liou, J.-C. Wang, *Inorg. Chem.*, 2001, **40**, 6499.
- 16 E. Zintl, K. Loosen, *Z. Phys. Chem.* 1935, **A 174**, 301.
- 17 W. Büsssem, H. Fischer, E. Gruner, *Naturwissenschaften*, 1935, **23**, 740.
- 18 S. Uhlandt, G. Meyer, *J. Alloys Compd.* 1995, **225**, 171;
- 19 C. M. Schurz, Th. Schleid, *J. Alloys Compd.* 2009, **485**, 110.
- 20 F. Lissner, Th. Schleid, *Z. anorg. allg. Chem.* 2005, **631**, 1119.
- 21 C. M. Schurz, Th. Schleid, *J. Solid State Chem.* 2010, **183**, 2253.
- 22 A. Olejniczak, A. Katrusiak, *CrystEngComm*, 2010, **12**, 2528.
- 23 Q. Hou, J.-J. Zhao, T.-Q. Zhao, J. Jin, J.-H. Yu, J.-Q. Xu, *J. Solid State Chem.*, 2011, **184**, 1756;
- 24 H. Chan, Y. Chen, M. Dai, C.-N. Lü, H.-F. Wang, Z.-G. Ren, Z.-J. Huang, C.-Y. Ni, J.-P. Lang, *CrystEngComm*, 2012, **14**, 466.
- 25 Q. Hou, X.-J. Qu, J. Jin, J.-J. Zhao, J.-H. Yu, J.-Q. Xu, *J. Cluster Sci.* 2011, **22**, 715.
- 26 J. Song, Y. Hou, L. Zhang, Y. Fu, *CrystEngComm*, 2011, **13**, 3750.
- 27 J.-J. Hou, S.-L. Li, C.-R. Li, X.-M. Zhang, *Dalton Trans.* 2010, **39**, 2701-2707.
- 28 N. P. Rath, E. M. Holt, *Inorg. Chem.*, 1985, **24**, 3934.
- 29 M. Vitale, W. E. Palke, P. C. Ford, *J. Phys. Chem.* 1992, **96**, 8329.
- 30 P. C. Ford, A. Vogler, *Acc. Chem. Res.*, 1993, **26**, 220.
- 31 P. C. Ford, E. Cariati, J. Bourassa, *Chem. Rev.* 1999, **99**, 3625.
- 32 M. Vitale, P. C. Ford, *Coord. Chem. Rev.* 2001, **219-221**, 3-16.
- 33 C. K. Ryu, M. Vitale, P. C. Ford, *Inorg. Chem.* 1993, **32**, 869.
- 34 E. Cariati, J. Bourassa, *Chem. Commun.* 1998, 1623.
- 35 E. Cariati, X. Bu, P. C. Ford, *Chem. Mater.* 2000, **12**, 3385.
- 36 M. J. Leitzl, F.-R. Kuchle, H. A. Mayer, L. Wesemann, H. Yersin, *J. Phys. Chem. A* 2013, **117**, 11823-11836.
- 37 D. M. Zink, M. Bächle, T. Baumann, M. Nieger, M. Kühn, C. Wang, W. Klopfer, U. Monkowius, T. Hofbeck, H. Yersin, S. Bräse, *Inorg. Chem.* 2013, **52**, 2292-2305
- 38 Liu, Z.; Djurovich, P. I.; Whited, M. T.; Thompson, M. E., *Inorg. Chem.* 2012, **51**, 230-6.
- 39 Wallesch, M.; Volz, D.; Zink, D. M.; Schepers, U.; Nieger, M.; Baumann, T.; Bräse, S., *Chemistry – A European Journal* 2014, **20**, 6578.
- 40 Liu, Z.; Qiu, J.; Wei, F.; Wang, J.; Liu, X.; Helander, M. G.; Rodney, S.; Wang, Z.; Bian, Z.; Lu, Z.; Thompson, M. E.; Huang, C., *Chem. Mater.* 2014, **26**, 2368.
- 41 Tsuge, K., *Chem. Lett.* 2013, **42**, 204-208.
- 42 P. C. Ford, *Coord. Chem. Rev.* 2011, **132**, 129-140.
- 43 R. Czerwieniec, J. Yu, H. Yersin, *Inorg. Chem.* 2011, **50**, 8293-8301;
- 44 H. Yersin, A. F. Rauch, R. Czerwieniec, T. Hofbeck, T. Fischer, *Coord. Chem. Rev.* 2011, **255**, 2622-2652.
- 45 Czerwieniec, R.; Kowalski, K.; Yersin, H., *Dalton Trans.* 2013, **42**, 9826-30.
- 46 X. Liu, G.-C. Guo, A.-Q. Wu, L.-Z. Cai, J.-S. Huang, *Inorg. Chem.* 2005, **44**, 4282-4286.
- 47 Cheng, J.-K.; Yao, Y.-G.; Zhang, J.; Li, Z.-J.; Cai, Z.-W.; Zhang, X.-Y.; Chen, Z.-N.; Chen, Y.-B.; Kang, Y.; Qin, Y.-Y.; Wen, Y.-H., *J. Am. Chem. Soc.* 2004, **126**, 7796-7797.
- 48 Bayse, C.; Harper, L. K.; Ming, J. L.; Pike, R. D., *Dalton Trans.* 2014, **43**, 11243-11251.
- 49 A. Pfitzner, *Chem. Eur. J.* 2000, **6**, 1891.
- 50 M. Andrzejewski, A. Olejniczak, A. Katrusiak, *Cryst. Growth Des.* 2011, **11**, 4892.
- 51 S. Maderlehner, A. Pfitzner, *Z. Kristallogr.* 2012, **227**, 569.
- 52 X-RED32, STOE & Cie GmbH, Darmstadt, 2004, X-SHAPE, STOE & Cie GmbH, Darmstadt, 1999.
- 53 A. Altomare, G. Cascarano, C. Giacovazzo, A. Gualardi, *J. Appl. Cryst.* 1993, **26**, 343.
- 54 G. M. Sheldrick, *Acta Crystallogr., Sect. A*, 2008, **64**, 112.
- 55 CrysAlisPro software, Agilent Technologies, Version 1.171.35.11, 2011.
- 56 Resolutions Pro software, Molecular Spectroscopy Solutions, Varian Inc., Version 4.1.0.101, 2006.
- 57 J. K. Nagle, *J. Am. Chem. Soc.*, 1990, **112**, 4741; A. Bondi, *J. Phys. Chem.* 1964, **68**, 441-451.
- 58 W. L. Bragg, *Philosophical Magazine*, 1914, **28**, 255.
- 59 A. K. Nurtaeva, E. M. Holt, *Acta Crystallogr., Sect. C*, 1998, **54**, 594.
- 60 H. Hartl, F. Mahdjour-Hassan-Abadi, *Angew. Chem.* 1981, **93**, 804. *Angew. Chem. Int. Ed.* 1981, **20**, 772.
- 61 S. Andersson, S. Jagner, *Acta Chem. Scand., Sect. A*, 1985, **39**, 181.
- 62 W. Wang, L. Zhang, X.-B. Xu, Q. Ye, *Inorg. Chem. Commun.* 2011, **14**, 626-631.
- 63 U. Müller, *Inorganic Structural Chemistry*, 2007, **2<sup>nd</sup> Edition**, John Wiley & Sons Ltd., The Atrium, Southern Gate, Chichester, West Sussex PO19 85Q, England.
- 64 E. Jalilian, S. Lidin, *CrystEngComm*, 2011, **13**, 5730.
- 65 S. Andersson, M. Håkansson, S. Jagner, *Inorg. Chim. Acta*, 1993, **209**, 195.
- 66 S. Lorenzo, C. Horn, D. Craig, M. Scudder, I. Dance, *Inorg. Chem.* 2000, **39**, 401.
- 67 A. Vogler, H. Kunkely, *J. Am. Chem. Soc.* 1986, **108**, 7211-7212.
- 100 M. J. Leitzl, V. A. Krylova, P. I. Djurovich, M. E. Thompson, H. Yersin, *J. Am. Chem. Soc.* 2014, **136**, 16032-16038.
- 101 R. Czerwieniec, H. Yersin, *Inorg. Chem.* 2015, **54**, 4322-4327.
- 102 C. Linfoot, M. J. Leitzl, P. Richardson, A. F. Rausch, O. Chepelin, F. J. White, H. Yersin, N. Robertson, *Inorg. Chem.* 2014, **53**, 10854-10861.
- 103 T. Hofbeck, U. Monkowius, H. Yersin, *J. Am. Chem. Soc.* 2015, **137**, 399.
- 104 F. Wu, J. Li, H. Tong, Z. Li, C. Adachi, A. Langlois, P. D. Harvey, L. Liu, W.-Y. Wong, W.-K. Wong, X. Zhu, *J. Mater. Chem. C* 2015, **3**, 138-146.
- 105 F. Wu, H. Tong, Z. Li, W. Lei, L. Liu, W.-Y. Wong, W.-K. Wong, X. Zhu, *Dalton Trans.* 2014, **43**, 12463-66.
- 106 D. L. Dexter, J. H. Schulman, *J. Chem. Phys.* 1954, **22**, 1063-1070.
- 107 G. Zeng, S. Xing, X. Han, B. Xin, Y. Yang, X. Wang, G. Li, Z. Shi, S. Feng, *R. Soc. Chem. Adv.* 2015, **5**, 40792-40797.
- 108 Y. Song, R. Fan, P. Wang, X. Wang, S. Gao, X. Du, Y. Yang, T. Luan, *J. Mater. Chem. C* 2015, **3**, 6249-6259.
- 109 M. Knorr, A. Bonnot, A. Lapprand, A. Khatyr, C. Strohmman, M. M. Kubicki, Y. Rousselin, P. D. Harvey, *Inorg. Chem.* 2015, **54**, **8**, 4076-4093.

**Table 1.** Crystal data and structure refinement for **1** and **2**

Compound	<b>1</b>	<b>2</b>
Empirical Formula	Br <sub>4</sub> C <sub>8</sub> Cu <sub>2</sub> H <sub>18</sub> N <sub>2</sub>	C <sub>8</sub> Cu <sub>2</sub> H <sub>18</sub> I <sub>4</sub> N <sub>2</sub>
Formula weight	588.96	776.92
Crystal system	monoclinic	monoclinic
Space group	<i>P</i> 2 <sub>1</sub> / <i>m</i> (No. 14)	<i>P</i> 2 <sub>1</sub> (No. 4)
Unit cell dimensions <sup>a</sup>	<i>a</i> = 9.169(4) Å <i>b</i> = 10.916(6) Å; $\beta$ = 93.93(2)° <i>c</i> = 15.349(6) Å	<i>a</i> = 15.8121(2) Å <i>b</i> = 9.4130(1) Å, $\beta$ = 90.011(1)° <i>c</i> = 22.9117(3) Å
Volume, <i>Z</i>	1533(2) Å <sup>3</sup> , 4	3410.16(7) Å <sup>3</sup> , 8
Crystal size / mm <sup>3</sup>	0.2 x 0.1 x 0.07	0.25 x 0.2 x 0.15
Density $\rho_{\text{calc}}$	2.552 g/cm <sup>3</sup>	3.027 g/cm <sup>3</sup>
Absorption coefficient $\mu(\text{MoK}\alpha)$	13.179 mm <sup>-1</sup>	9.717 mm <sup>-1</sup>
Temperature	293 K	123 K
<i>F</i> <sub>000</sub>	1112	2800
$\theta$ range for data collection	2.29 to 25.45°	3.08 to 28.70°
Limiting indices	-11 ≤ <i>h</i> ≤ 11, -13 ≤ <i>k</i> ≤ 13, -18 ≤ <i>l</i> ≤ 18	-21 ≤ <i>h</i> ≤ 21, -12 ≤ <i>k</i> ≤ 11, -30 ≤ <i>l</i> ≤ 27
Reflections collected	18384	21747
Independent reflections	2821 [ <i>R</i> <sub>int</sub> = 0.0501]	14978 [ <i>R</i> <sub>int</sub> = 0.0273]
Data / restraints / parameters	2821 / 0 / 199	14978 / 1 / 388
Goof <i>S</i>	1.040	1.038
Final <i>R</i> indices [ <i>I</i> > 2σ( <i>I</i> )]	<i>R</i> <sub>1</sub> = 0.0326, <i>wR</i> <sub>2</sub> = 0.0665	<i>R</i> <sub>1</sub> = 0.0337, <i>wR</i> <sub>2</sub> = 0.0756
<i>R</i> indices (all data)	<i>R</i> <sub>1</sub> = 0.0457, <i>wR</i> <sub>2</sub> = 0.0698	<i>R</i> <sub>1</sub> = 0.0340, <i>wR</i> <sub>2</sub> = 0.0759
Weighting coefficients	<i>a</i> = 0.0394, <i>b</i> = 0	<i>a</i> = 0.0302, <i>b</i> = 0
$\Delta\rho_{\text{min}}, \Delta\rho_{\text{max}} / \text{e}\text{\AA}^{-3}$	0.629, -0.482	1.078, -1.048
Flack parameter	-	0.00

a) lattice constants of **1** were refined from powder diffraction data (PLEASE PRINT OVER TWO COLUMNS)

**Table 2.** Structural details of the tetrahedral chains  $^1[\text{Cu}_2\text{X}_4^{2-}]$  and  $^1[\text{N}_2\text{RE}_4^{6+}]$ , respectively

Compound/ cation [reference]	<i>d</i> (Cu-X) / Å	<i>d</i> (Cu-Cu) / Å	$\angle$ (X-Cu-X) / °	$\angle$ (Cu-X-X-Cu <sup>a</sup> ) / °	<i>d</i> (X-X <sup>b</sup> ) / Å	<i>d</i> (X-X <sup>c</sup> ) / Å
<b>1</b>	2.492-2.575	2.740-2.970	102-118	119	3.99-4.35	3.874
<b>2</b>	2.643-2.706	2.679-3.352	101-120	117-121	4.099-4.624	4.059-4.139
NH <sub>4</sub> <sup>+</sup> [4]	2.631-2.697	2.809, 3.102	106-117	132-160	4.239-4.496	4.424-5.650
Rb <sup>+</sup> [4]	2.628-2.715	2.897, 3.098	107-118	133-157	4.281-4.518	4.511-5.730
<i>N</i> -allyl-quinolinium [6]	2.50-2.623	3.305, 3.620	91-124	155	3.649-4.42	6.243
La <sub>4</sub> N <sub>2</sub> Te <sub>3</sub> [11]	2.337-2.371	3.029, 3.106	96-118	146	3.525-4.070	4.718

a) Dihedral angle at the kinked junction; b) within the CuX<sub>4</sub> tetrahedra; c) between neighboring CuX<sub>4</sub> tetrahedra; (X = Br, I), see Figure 2. (PLEASE PRINT OVER TWO COLUMNS)



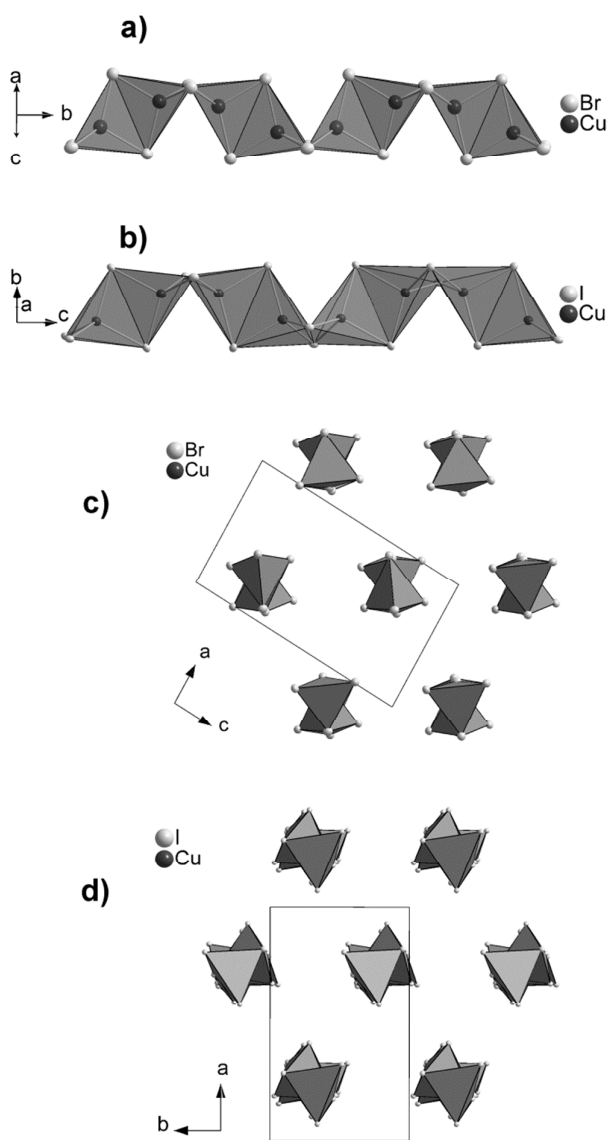


**Figure 1.**  $\text{Cu}_2\text{X}_4$  chains ( $\text{X} = \text{Br}$ ,  $\text{I}$ ) in **1 a)** and **2 b)** showing the strong kinking. Projections are displayed in **1 c)** and **2 d)** showing the hexagonal packing of the chains and the AB-stacking of two different orientations in **2**

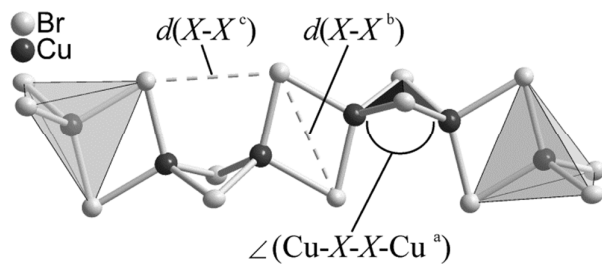


**Figure 2.** Section of the chain structure in **1**. Distances and angles given in Table 2 are labeled.

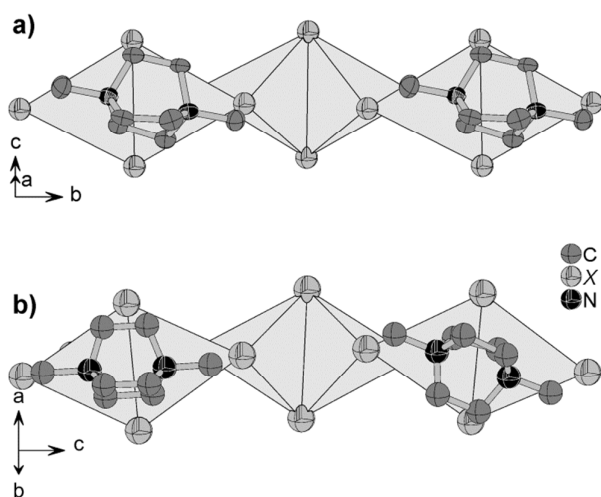


**Figure 3.** Orientation of the cations in **1** (X = Br) a) and **2** (X = I) b) relative to the anionic chain structure, showing two alternating orientations in **2**. Hydrogen atoms omitted for clarity.

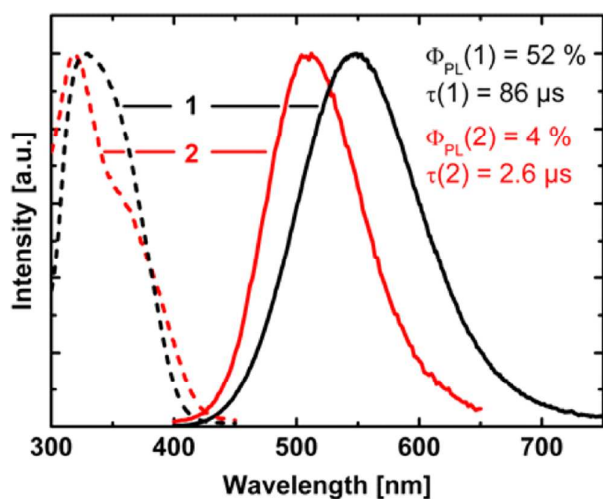


**Figure 4.** Emission (solid lines) and excitation (dotted lines) spectra of **1** [DABCOMe<sub>2</sub>][Cu<sub>2</sub>Br<sub>4</sub>] (black) and **2** [DABCOMe<sub>2</sub>][Cu<sub>2</sub>I<sub>4</sub>] (red). The spectra were recorded from powders of the substances at ambient temperature ( $\lambda_{\text{exc}} = 350$  nm).  $\Phi_{\text{PL}}$  represents the emission quantum yield and  $\tau$  the emission decay time.

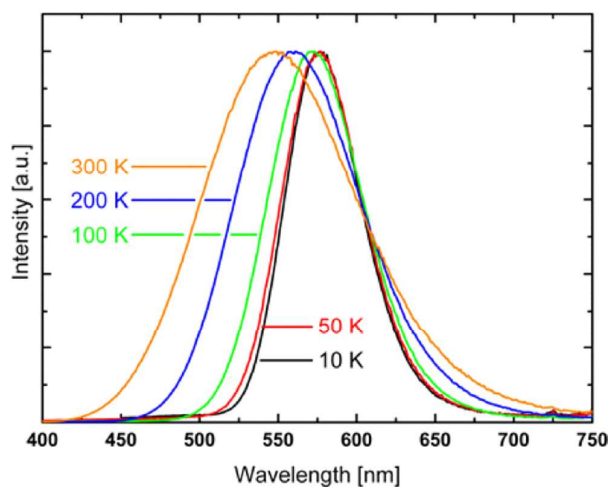


**Figure 5.** Emission spectra of [DABCOMe<sub>2</sub>][Cu<sub>2</sub>Br<sub>4</sub>] (**1**) at different temperatures. Excitation wavelength  $\lambda_{\text{exc}} = 350$  nm

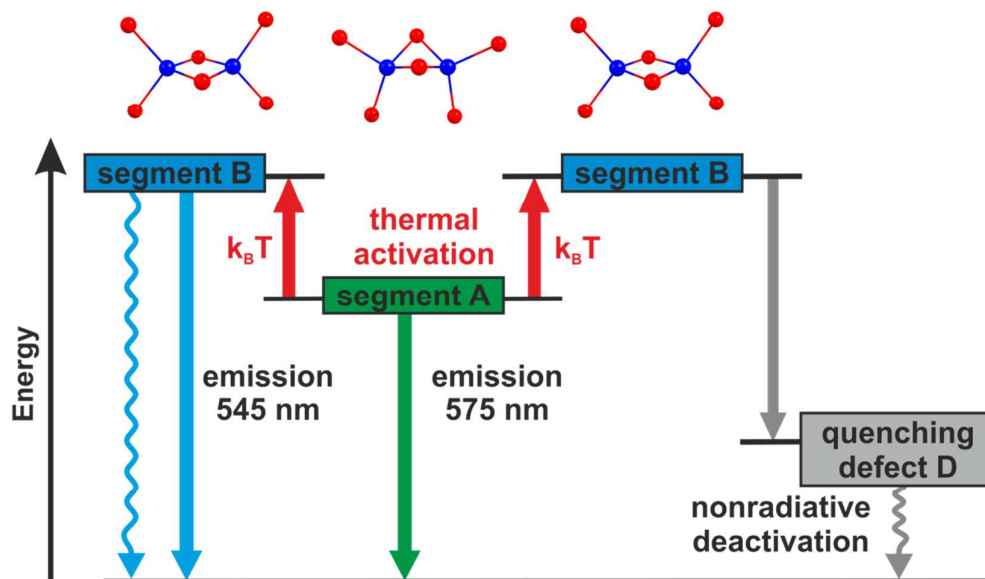


**Figure 6.** Scheme of a proposed emission and quenching mechanism referring to compound **1**. At low temperatures ( $< 50$  K), only the energetically lower lying chain segments **A** emit. With increasing temperature, **B** segments can be thermally populated and emit at higher energy ( $\approx 10^3$   $\text{cm}^{-1}$ ). However, according to the proposed mechanism, energy can also be transferred along chain segments and thus, reach unavoidable defect sites where the excitation can be deactivated nonradiatively. The structures of the respective chain segment types are displayed above the energy level diagram. Hereby, blue and red spheres represent copper and bromide atoms, respectively.

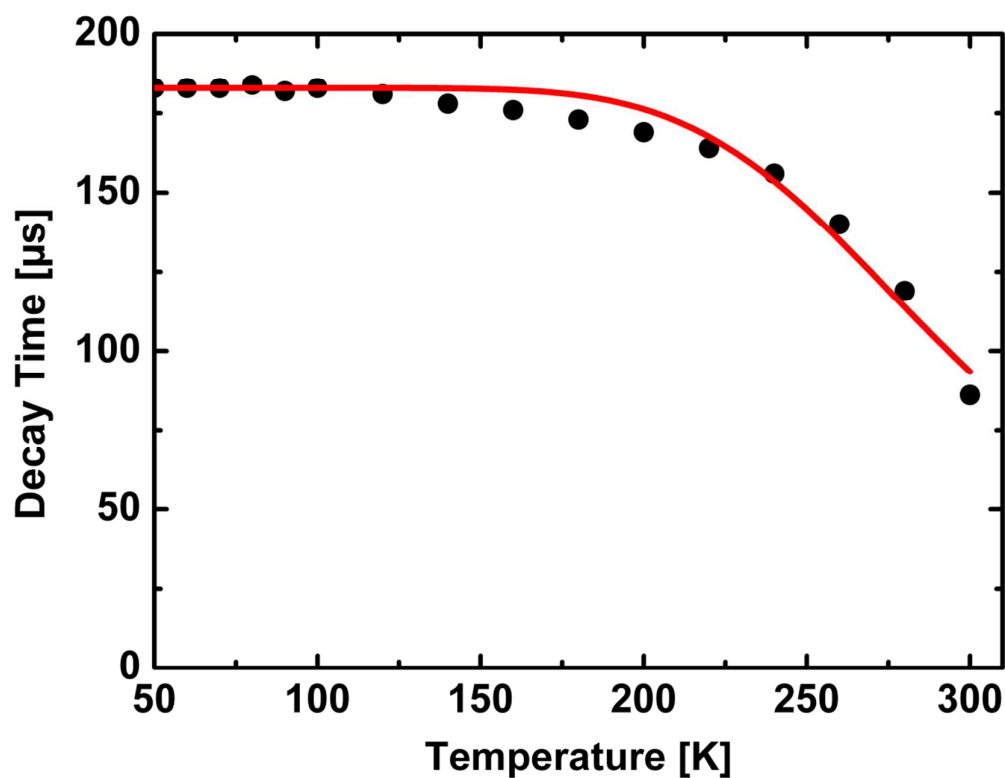
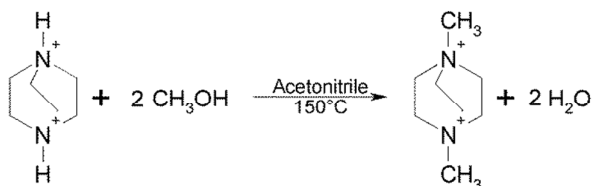


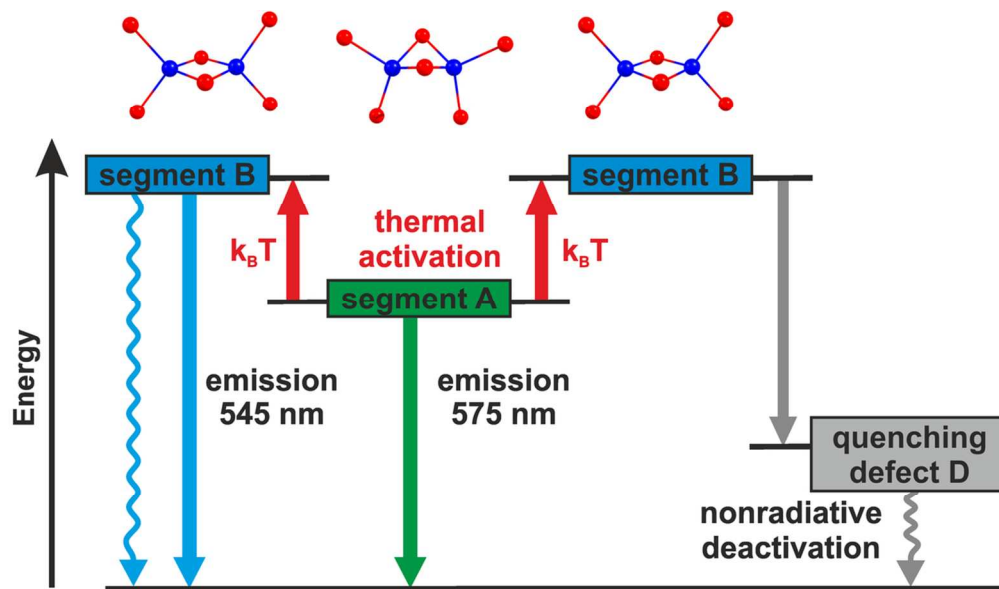
**Figure 7:** Temperature dependent emission decay time of [DABCOMe<sub>2</sub>][Cu<sub>2</sub>Br<sub>4</sub>] (1). As excitation light source a Nd:YAG laser with a wavelength of 355 nm was used. The red line represents a fit according to eq. (1).

Equation (1)

$$\tau(T) = \frac{1 + \exp\left[-\frac{\Delta E(A-B)}{k_B T}\right]}{\frac{1}{\tau(A)} + \left(\frac{1}{\tau(B)} + \frac{1}{\tau(D)}\right) \exp\left[-\frac{\Delta E(A-B)}{k_B T}\right]}$$



**Scheme 1.** Twofold *N*-methylation of DABCO by methanol



106x61mm (300 x 300 DPI)